MCB
Journals.ASM.org

Deficiency of a Lipid Droplet Protein, Perilipin 5, Suppresses Myocardial Lipid Accumulation, Thereby Preventing Type 1 Diabetes-Induced Heart Malfunction

Kenta Kuramoto,[a] Fumie Sakai,[a] Nana Yoshinori,[a] Tomoe Y. Nakamura,[b] Shigeo Wakabayashi,[b] Tomoko Kojidani,[c,d] Tokuko Haraguchi,[d,e,f] Fumiko Hirose,[a] Takashi Osumi[a]

Graduate School of Life Science, University of Hyogo, Kamigori, Hyogo, Japan[a]; Department of Molecular Physiology, National Cerebral and Cardiovascular Center Research Institute, Suita, Osaka, Japan[b]; Department of Chemical and Biological Science, Japan Women's University, Bunkyo-ku, Tokyo, Japan[c]; Advanced ICT Research Institute Kobe, National Institute of Information and Communication Technology, Nishi-ku, Kobe, Japan[d]; Graduate School of Frontier Bioscience, Osaka University, Suita, Osaka, Japan[e]; Graduate School of Science, Osaka University, Toyonaka, Japan[f]

Lipid droplet (LD) is a ubiquitous organelle that stores triacylglycerol and other neutral lipids. Perilipin 5 (Plin5), a member of the perilipin protein family that is abundantly expressed in the heart, is essential to protect LDs from attack by lipases, including adipose triglyceride lipase. Plin5 controls heart metabolism and performance by maintaining LDs under physiological conditions. Aberrant lipid accumulation in the heart leads to organ malfunction, or cardiomyopathy. To elucidate the role of Plin5 in a metabolically disordered state and the mechanism of lipid-induced cardiomyopathy, we studied the effects of streptozotocin-induced type 1 diabetes in *Plin5*-knockout (KO) mice. In contrast to diabetic wild-type mice, diabetic *Plin5*-KO mice lacked detectable LDs in the heart and did not exhibit aberrant lipid accumulation, excessive reactive oxygen species (ROS) generation, or heart malfunction. Moreover, diabetic *Plin5*-KO mice exhibited lower heart levels of lipotoxic molecules, such as diacylglycerol and ceramide, than wild-type mice. Membrane translocation of protein kinase C and the assembly of NADPH oxidase 2 complex on the membrane were also suppressed. The results suggest that diabetic *Plin5*-KO mice are resistant to type 1 diabetes-induced heart malfunction due to the suppression of the diacylglycerol/ceramide-protein kinase C pathway and of excessive ROS generation by NADPH oxidase.

The heart normally obtains 60 to 70% of its necessary energy through fatty acid (FA) β-oxidation (1). On the other hand, aberrant lipid accumulation occurs in the heart in cases of obesity and diabetes due to increased FA influx (2, 3). Excess FAs are converted to triacylglycerol (TAG) and stored in lipid droplets (LDs), which are metabolically active organelles surrounded by a monolayer of phospholipids and which occur in almost all tissues (4, 5). Compared with LDs in white adipose tissue, heart LDs are much smaller, and the lipid contents are turned over much faster.

Many proteins are located on LD surfaces, likely contributing to the properties of LDs (4). Perilipin (Plin) family proteins form a group of representative LD-associated proteins, composed of five members, Plin1 to Plin5 (6, 7). Plin1 and Plin4 are expressed mainly in adipose tissues, whereas Plin2 and Plin3 are found in a wide variety of tissues. Unlike other Plin family proteins, Plin5 is expressed abundantly in oxidative tissues, particularly in the heart (8–10). We previously found that detectable LDs are lost in the hearts of *Plin5*$^{-/-}$ mice, and we demonstrated that Plin5 is essential to protect heart LDs from attack by adipose triglyceride lipase (ATGL) and/or a related lipase(s). Because FAs are not sequestered as TAG in LDs, larger amounts of FAs are oxidized in mitochondria in the hearts of *Plin5*$^{-/-}$ mice, leading to excess generation of reactive oxygen species (ROS), which causes an eventual age-dependent decrease in heart function. Thus, heart LDs serve to limit oxidative damage of the heart by regulating FA influx into the mitochondrial oxidation pathway (11).

Intramyocardial TAG levels are inversely correlated with heart function, and chronic lipid accumulation leads to heart malfunction (2, 3, 12). Diabetic patients often suffer from a diabetes-induced decline in heart function, which is called diabetic cardiomyopathy (13). Simultaneous accumulation of LDs manifests in the hearts of these patients (14, 15). Hence, abnormal lipid metabolism, including aberrant lipid accumulation, is regarded as an important pathogenesis of diabetic cardiomyopathy. Efforts have been made to elucidate the link between lipid metabolism and heart performance using obese and diabetic mouse models as well as genetically modified mice (16–24). Previous studies focusing on abnormal lipid metabolism suggest two causes for major pathogenesis of diabetes-induced heart malfunction. One cause is augmentation of oxidative stress due to enhanced mitochondrial ROS generation caused by excess FA oxidation (25–27). The other is excess accumulation of lipotoxic molecules, such as diacylglycerol (DAG) and ceramide, which disrupt several signaling pathways, including the protein kinase C (PKC) pathway (19, 28, 29). However, it is not clear which of the two proposed causes primarily contributes to the development of diabetic cardiomyopathy.

Based on the essential function of Plin5 in maintaining LDs in the heart under physiological conditions, we expected that this protein also would play a critical role in aberrant heart lipid accumulation under pathological conditions. Accordingly, we generated type 1 diabetic *Plin5*$^{-/-}$ mice by treatment with streptozoto-

Received 25 January 2014 **Returned for modification** 28 February 2014
Accepted 6 May 2014
Published ahead of print 12 May 2014
Address correspondence to Takashi Osumi, osumi@sci.u-hyogo.ac.jp.

doi:10.1128/MCB.00133-14

TABLE 1 Primer sequences used for PCR

Gene description (name)[a]	Forward primer sequence (5′→3′)	Reverse primer sequence (5′→3′)
Perilipin 2 (*Plin2*)	CTCAGGAGGAGCTGGAGATG	TCAATCAGGTGGACAGTGGA
Perilipin 3 (*Plin3*)	CCATGTCTAGCAATGGTACAG	GACACCAGTTCCTTAGTATCC
Perilipin 4 (*Plin4*)	GACAACTGAGGAACAAGCTCAG	TCCATGGTCATGTCTGTCATCT
Perilipin 5 (*Plin5*)	CCTTGCTGAGCACTGTGTGT	TGCTAGCTCAGCCTCAGTCA
Collagen type 1 alpha 2 (*Col1a2*)	TGGCCCATCTGGTAAAGAAG	ACCTTTGCCACCTTGAACAC
Cluster of differentiation 36 antigen (*CD36*)	CCATTGGTGATGAAAAAGCA	GATCGGCTTTACCAAAGATGTAG
Lipoprotein lipase (*LPL*)	TCGTCATCGAGAGGATCCGA	TGTTTGTCCAGTGTCAGCCA
Solute carrier family 27, member 1 (*Slc27a1*)	TTCTCGTGGGCCAGATCAAC	GCACGTCACCTGAGAGGTAG
Solute carrier family 27, member 6 (*Slc27a6*)	GGAGAAAACGTCGCAACCAC	CCTTCATAACCTGGCACACG
Glutamate oxaloacetate transaminase 2 (*GOT2*)	GCCAAGAACATGGGCCTGTA	CTTGCAACCATTGCTTCCGC
Ribosomal protein large P0 (*Rplp0*)	TTCGTGTTCACCAAGGAGGAC	ATGATCAGCCCGAAGGAGAAG

[a] *Slc27a1* and *Slc27a6* code for fatty acid transport protein 1 (FATP1) and FATP6, respectively. GOT2 is identical to plasma membrane fatty acid-binding protein (FABPpm).

cin (STZ) and compared their phenotypes with those of diabetic wild-type (WT) mice. As expected, diabetic *Plin5*$^{-/-}$ mice lacked heart LDs and were resistant to lipid-induced heart malfunction. Here, we describe the underlying mechanism that, in turn, sheds light on the pathogenesis of diabetic cardiomyopathy.

MATERIALS AND METHODS

Mice. *Plin5*$^{-/-}$ mice were generated in our laboratory, as described previously (11), and were backcrossed to the C57BL/6J background for 10 generations. The *Plin5*$^{-/-}$ mouse strain was donated to RIKEN Bioresource Center, Japan, under identification number RBRC05649. *Plin5*$^{+/+}$ and *Plin5*$^{-/-}$ mice used for experiments were obtained by breeding homozygous parents. C57BL/6J (WT), *Lepr*^{db}/*Lepr*^{db} (leptin receptor deficiency), and lean control *Lepr*$^{db/+}$ mice were obtained from CLEA Japan. Type 1 diabetic *Ins2*$^{WT/C96Y}$ (Akita) mice were obtained from Japan SLC.

Diet-induced obese mice were obtained by feeding the mice from ages 3 to 4 to 18 to 20 weeks with a high-fat diet (60% of calories from fat) (HFD32; CLEA Japan).

STZ-induced diabetic mice were generated as follows. Mice at 10 to 14 weeks of age were intraperitoneally injected with STZ (Nacalai Tesque) in saline at a dose of 150 mg/kg body weight every 3 to 4 days until blood glucose concentration exceeded 350 mg/dl. Blood glucose levels were measured with a Glutest sensor (SKK). Eight weeks after diabetes was established, mice were used for experiments. Some animals were treated with *N*-acetyl-L-cysteine (NAC) (Wako) at a dose of 500 mg/kg/day as described previously (11) for 8 weeks after onset of diabetes.

The mice were housed on a regular 12-h light/dark cycle and were fed with a standard chow diet (CA-1; CLEA Japan) and water *ad libitum*. All the animal procedures were conducted according to the guidelines of University of Hyogo for the care and use of experimental animals.

Reverse transcription-PCR (RT-PCR). Total RNA was isolated from the left ventricle using a QIAzol lysis reagent (Qiagen), according to the manufacturer's protocol. For first-strand cDNA synthesis, 2 μg of total RNA was reverse transcribed at 37°C for 1 h using random hexamer primers (TaKaRa) and Moloney murine leukemia virus (M-MLV) reverse transcriptase (Invitrogen). Target genes were amplified with a *Taq* DNA polymerase (KAPA) using specific primer sets (Table 1). The PCR products were separated in 2% agarose gels containing ethidium bromide and detected by a luminescence image analyzer (LAS-1000; Fujifilm). The intensities of specific bands were quantified using ImageJ software.

qPCR. cDNA templates were prepared as described above. Quantitative PCR (qPCR) was performed in a CFX96 real-time detection system (Bio-Rad) using SsoAdvanced SYBR green Supermix (Bio-Rad) and specific primer sets (Table 1). Relative mRNA levels were quantified using the comparative threshold cycle (C_T) method and normalized to *Rplp0* mRNA levels.

Immunoblot analysis. Tissues were homogenized using a Polytron homogenizer (Kinematica AG) in a lysis buffer (20 mM Tris-HCl [pH 7.5], 1% Nonidet P-40, 0.5% sodium deoxycholate, 1% SDS, 150 mM NaCl, 10 mM NaF, 1 mM sodium pyrophosphate, 1 mM sodium orthovanadate, a protease inhibitor cocktail [Roche], and 1 mM EDTA). Protein concentration was determined using a protein assay kit (Bio-Rad). Samples containing equivalent amounts of protein were resolved by SDS-PAGE and transferred to polyvinylidene difluoride or nitrocellulose membranes. Proteins were probed using the following antibodies: Plin5 (developed in-house [8] and by Progen [GP31]); Plin2 (GP40; Progen); Plin3 (3883; Prosci); ATGL (2138), phospho-p38 (4511), and p38 (9212) (Cell signaling); pan-cadherin (C3678), PKC (P5704), and p47^{phox} (SAB4502810) (Sigma); glyceraldehyde-3-phosphate dehydrogenase (GAPDH) (sc-25778) and β-tubulin (sc-9104) (Santa Cruz); hormone-sensitive lipase (HSL) (ab45422) and uncoupling protein 3 (UCP3) (ab3477) (Abcam); p67^{phox} (610912; BD Bioscience); and acyl coenzyme A (CoA) oxidase (Acox), very long-chain acyl-CoA dehydrogenase (VLCAD), and medium-chain acyl-CoA dehydrogenase (MCAD) (gifts from T. Hashimoto and S. Yamaguchi). Horseradish peroxidase (HRP)-conjugated secondary antibodies were anti-rabbit (NA934) and mouse (NA931) (GE Healthcare) and anti-guinea pig (AP108P [Chemicon] and sc-2438 [Santa Cruz]) antibodies. Specific bands were visualized by chemiluminescence with an X-ray film (Fujifilm) and were quantified using ImageJ software.

Biochemical analyses. Total lipids were extracted from the left ventricle by the Folch method. TAG and FA levels in total lipid extracts or plasma samples were measured by colorimetric methods, using a triglyceride Etest (Wako) and nonesterified fatty acid C-test (Wako), respectively. Plasma total cholesterol and free cholesterol were determined with a cholesterol Etest and free-cholesterol Etest (Wako), respectively. Plasma glucose levels were determined by a glucose CII test (Wako), and plasma insulin levels were quantified by an insulin enzyme-linked immunosorbent assay (ELISA) kit (Shibayagi).

Electron microscopy. Electron microscopy was performed as described previously (11). Briefly, left ventricle tissue pieces were prefixed with 2% glutaraldehyde in 0.1 M sodium phosphate buffer (PB; pH 7.4) overnight at 4°C, washed with PB, and postfixed with 2% osmium tetroxide in PB at 4°C for 2 h. Ultrathin sections were stained with 2% uranyl acetate solution and lead stain solution (Sigma). Samples were observed using an electron microscope (JEM1200EX; JEOL) at 80 kV.

Immunofluorescence staining. Tissues were fixed with 10% formalin in phosphate-buffered saline (PBS). Preparation of cryosections and immunofluorescence staining were performed as described previously (11). Sections were permeabilized with methanol at −20°C for 20 min and blocked with 2% bovine serum albumin (BSA)-PBS for 1 h at room temperature. Sections were then incubated with primary antibodies against Plin2 (raised in guinea pig) (GP40; Progen) overnight at 4°C, washed with PBS, and incubated with a secondary antibody, Alexa Fluor 546-conjugated anti-guinea pig IgG (Invitrogen), at room temperature for 1 h. Sam-

ples were observed by confocal laser scanning microscopy (LSM510; Zeiss).

Immunoelectron microscopy. For preembedding immunoelectron microscopy, the heart was perfused and fixed with 4% formaldehyde–0.025% glutaraldehyde in PBS, and 6-μm-thick frozen sections were prepared. Sections were blocked and permeabilized with 1% BSA–1% saponin in PB for 1 h. Sections were incubated with a primary antibody against Plin2 (ab108323; Abcam) overnight at 4°C, washed with 0.005% saponin in PB, and incubated with a secondary antibody, Alexa Fluor 594 FluoroNanogold-conjugated anti-rabbit IgG (Nanoprobes), for 2 h. After samples were washed, sections were fixed with 1% glutaraldehyde in PB for 10 min, and silver enhancement was performed as described previously (30). Samples were then postfixed with 1% reduced osmium tetroxide, and ultrathin sections were prepared, followed by staining with 4% uranyl acetate and lead stain solution (Sigma). Samples were examined using an electron microscope (JEM1400; JEOL).

Measurement of DAG and ceramide contents. *sn*-1,2-DAG and ceramide contents were measured as described previously (31), using the total lipid extracts prepared as described above. Briefly, lipid extracts were incubated with 0.1 μmol of [γ-^{32}P]ATP (555 Bq/nmol) and *Escherichia coli* diacylglycerol kinase (Sigma) for 1 h at 27°C. This enzyme selectively phosphorylates *sn*-1,2-DAG among DAG isoforms. The reaction products were resolved on a thin-layer chromatography (TLC) plate, using the developing solvent chloroform-acetone-methanol-acetic acid-water (10:4:3:2:1, by volume). The TLC plate was exposed to an imaging plate (Fujifilm), and the radioactive spots corresponding to [^{32}P]phosphatidic acid and [^{32}P]ceramide-phosphate were detected by a Typhoon FLA 7000 (GE Healthcare), followed by quantification using Image Quant TL software (GE Healthcare).

TBARS assay. Malondialdehyde (MDA) content in the heart was measured by a thiobarbituric acid reactive substance (TBARS) assay as described previously (11), except that the reaction products were quantified fluorometrically. Measurement was performed in a fluorescence spectrophotometer (RF-5300PC; Shimadzu) at 536-nm excitation and 551-nm emission wavelengths.

Echocardiography. Echocardiography was performed on 1.5% isoflurane-anesthetized mice using Vevo 2100 (Visual Sonics), as described previously (11). The left ventricular fractional shortening (FS) was calculated as follows: $[(\mathrm{LVID}_d - \mathrm{LVID}_s)/\mathrm{LVID}_d] \times 100$, where LVID_d and LVID_s indicate the left ventricular internal end-diastolic and end-systolic dimensions, respectively.

Fractionation of the heart. Freshly isolated mouse hearts were washed with ice-cold PBS and homogenized in an ice-cold homogenization buffer (0.25 M sucrose, 20 mM Tris-HCl [pH 7.4], 1 mM EDTA, and a protease inhibitor cocktail [Roche]), using a Potter-Elvehjem Teflon homogenizer. Homogenates were centrifuged at 400 × *g* for 5 min at 4°C. The supernatants were transferred to new tubes, the homogenization was repeated three times for the precipitates, and the supernatants were combined. The supernatants were centrifuged at 5,500 × *g* for 10 min at 4°C, and the precipitates were suspended in a mitochondrion incubation buffer containing 30 mM HEPES (pH 7.4), 145 mM KCl, 5 mM KH_2PO_4, 3 mM $MgCl_2$, 0.1 mM EGTA, 0.1% FA-free BSA, and a protease inhibitor cocktail (Roche). Mitochondrial ROS generation capacity was measured for the mitochondrial suspension, as described below. The supernatant obtained above from centrifugation at 5,500 × *g* was further centrifuged at 100,000 × *g* for 1 h at 4°C in an ultracentrifuge (CS100GXL; Hitachi) using a swinging bucket rotor (S52ST; Hitachi), and the precipitates were used for an immunoblot assay as a membrane fraction.

Determination of hydrogen peroxide (H_2O_2) generation in mitochondria. H_2O_2 production was measured by H_2O_2-induced fluorescence of homovanillic acid as described previously (32). Briefly, a mitochondrial suspension (0.25 mg of protein/1.5 ml) was incubated with the reaction mixture containing 6 U/ml HRP, 0.1 mM homovanillic acid, 1 μg/ml oligomycin, and substrates (2.5 mM pyruvate–2.5 mM malate or 5 mM succinate) in the presence or absence of 2 μM rotenone for 15 min at 37°C. The reaction was stopped by the addition of 0.5 ml of stop solution, including 0.1 M glycine-NaOH (pH 12.0) and 25 mM EDTA, and the fluorescence was measured in a fluorescence spectrophotometer at 312-nm excitation and 420-nm emission wavelengths.

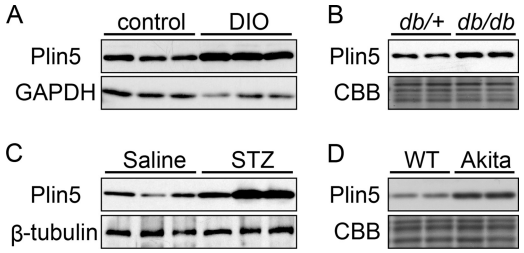

FIG 1 Plin5 protein levels increased in the hearts of mouse models for metabolic disorders. The Plin5 protein levels of DIO (A), *Lepr*^{db}/*Lepr*^{db} (db/db) (B), STZ-induced type 1 diabetic (C), and Akita (D) mice were examined by immunoblotting using total protein extracts of the heart. GAPDH, β-tubulin, or Coomassie brilliant blue (CBB) staining of the gel was used as a loading control.

Statistical analyses. All the data are shown as means ± standard errors of the means (SEM). Data were analyzed by Student's *t* test for comparisons between two groups and one-way analysis of variance, followed by Fisher's least-significant difference test for comparison between more than two groups. Differences with a *P* value of <0.05 were considered statistically significant. The correlation between FS and TBARS values was assessed by a regression analysis.

RESULTS

Involvement of Plin5 in heart TAG accumulation upon metabolic abnormalities. Plin5 is a critical protector of heart LDs against attack by lipases, and hence detectable LDs are lost in the heart with Plin5 deficiency at physiological states (11). On the other hand, the number of LDs and the TAG content in the heart increase with metabolic disorders, such as obesity and diabetes (2). Accordingly, we expected that Plin5 expression would be upregulated in the heart under these conditions. To assess this notion, we examined the amount of Plin5 protein in the hearts of the model mice with metabolic abnormalities, including diet-induced obesity (DIO), leptin receptor deficiency (*Lepr*^{db}/*Lepr*^{db}), STZ-induced type 1 diabetes, and genetic type 1 diabetes (*Ins2*$^{WT/C96Y}$ [Akita]) (Fig. 1). In all of these metabolically dysfunctional mice, Plin5 protein levels were elevated compared with those of the respective controls. For mice with STZ-induced diabetes, the levels of heart *Plin5* mRNA (see Fig. 4A and B) and protein (see Fig. 5A and B) were 1.9-fold and 2.0-fold higher, respectively, than those of nondiabetic (saline-treated) control mice. It should be noted that *Plin5* is a target gene of peroxisome proliferator-activated receptor α (PPARα), the targets of which are induced in obesity and diabetes (16, 26). Thus, *Plin5* is upregulated during metabolic disorders, suggesting the involvement of the protein in aberrant TAG accumulation under these conditions.

Because Plin5 is essential for maintaining heart LDs under physiological conditions, we expected that diabetes-induced aberrant lipid accumulation would also be prevented by Plin5 deficiency. Indeed, we found by electron microscopy that STZ-induced diabetic *Plin5*$^{-/-}$ mice lacked LDs in the heart, in contrast to the occurrence of numerous LDs in diabetic WT mice (Fig. 2A), as observed at physiological states. The morphologies of the mitochondria and actin-myosin filaments were indistinguishable between the two genotypes. Consistent with the different LD abun-

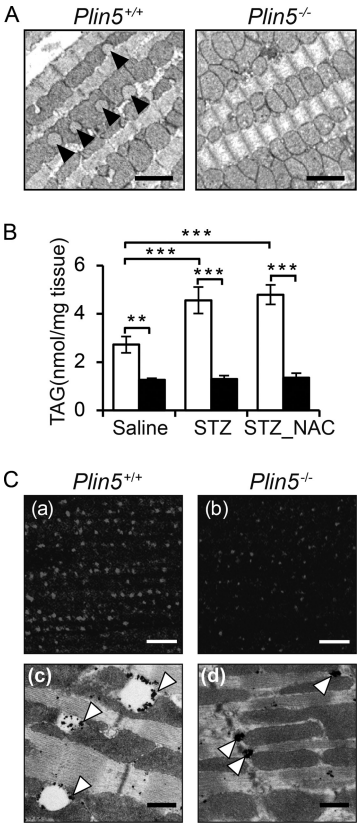

FIG 2 Aberrant TAG accumulation is suppressed in the hearts of *Plin5*$^{-/-}$ mice. (A) Representative electron micrograph of the hearts of STZ-induced diabetic WT mice and *Plin5*$^{-/-}$ mice. Arrowheads indicate LDs. Scale bars, 2 μm. (B) TAG contents in the hearts of saline-treated nondiabetic, STZ-treated diabetic, and STZ- and NAC-treated diabetic (STZ-NAC) mice. Open bars, WT mice; filled bars, *Plin5*$^{-/-}$ mice. Data are shown as means ± SEM (**, $P < 0.01$; ***, $P < 0.001$; $n = 5$ per group). (C) Representative images of immunofluorescence staining (a and b) and immunoelectron microscopy (c and d) of Plin2 in the hearts of diabetic mice. Scale bars, 5 μm (a and b) and 500 nm (c and d). Arrowheads indicate the Plin2-positive signals, which were discerned as heavy accumulations of silver grains, by comparison with the images of control samples processed in parallel without the primary antibody.

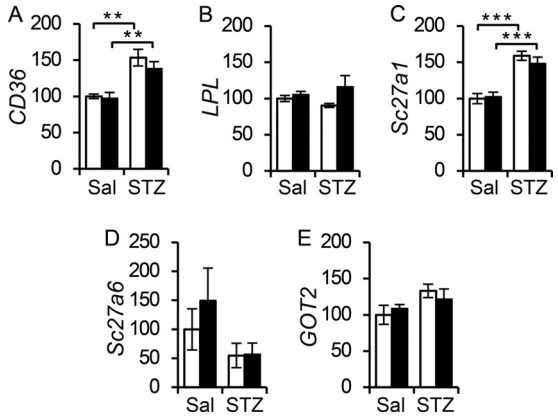

FIG 3 mRNA expression of *CD36* (A), *LPL* (B), *Slc27a1* (fatty acid transporter 1 [FATP1] gene) (C), *Slc27a6* (FATP6 gene) (D), and *GOT2* (plasma membrane fatty acid binding protein [FABPpm] gene) (E) in the hearts of nondiabetic and diabetic WT (open bars) and *Plin5*$^{-/-}$ (filled bars) mice ($n = 4$ per group). mRNA levels relative to those of saline-treated (Sal) control WT mice are presented. Data are shown as means ± SEM (**, $P < 0.01$; ***, $P < 0.001$).

dances, the heart TAG content increased in diabetic WT mice but not in *Plin5*$^{-/-}$ mice under the same conditions (Fig. 2B). We previously observed similar activities of FA uptake by cultured cardiomyocytes obtained from both genotypes of mice (11). Plasma levels of TAG, nonesterified FA, and total and free cholesterol were similar between the genotypes under normal and diabetic conditions (Table 2), except for higher free cholesterol in STZ-treated *Plin5*$^{-/-}$ mice. Heart expression levels of mRNAs involved in FA uptake (CD36, lipoprotein lipase, FA transport protein 1 [FATP1], FATP6, and plasma membrane FA binding protein [FABPpm]) were similar between the genotypes (Fig. 3). Expression of CD36 and FATP1 was upregulated in the diabetic state, representing increased FA uptake upon induction of diabetes. Thus, diminished TAG accumulation in the hearts of *Plin5*$^{-/-}$ mice is not likely to be due to the decrease in FA incorporation.

We previously showed the occurrence of minute LDs coated with Plin2, another Plin family protein, in the hearts of *Plin5*$^{-/-}$ mice (11). These structures are largely depleted of TAG due to Plin5 deficiency and are consequently undetectable by usual lipid staining or electron microscopy. Thus, most of the TAG remaining in the hearts of *Plin5*$^{-/-}$ mice conceivably is accommodated in

TABLE 2 Body weight, heart weight, and plasma levels of metabolites and insulin in WT mice and *Plin5*$^{-/-}$ mice

Parameter[a]	Value for the group by treatment[b]					
	Saline		STZ		STZ-NAC	
	Plin5$^{+/+}$	*Plin5*$^{-/-}$	*Plin5*$^{+/+}$	*Plin5*$^{-/-}$	*Plin5*$^{+/+}$	*Plin5*$^{-/-}$
Body wt (g)	29.67 ± 0.49	30.46 ± 0.72	21.89 ± 1.40***	22.31 ± 1.06***	21.07 ± 0.74***	21.13 ± 0.38***
Heart wt (mg)	116.75 ± 2.24	120.52 ± 5.20	74.45 ± 8.42***	83.31 ± 6.23***	80.71 ± 4.66***	77.35 ± 3.49***
Glucose (mM)	9.3 ± 05	8.8 ± 0.4	28.1 ± 0.4***	30.5 ± 1.6***	22.7 ± 1.2***, ##	24.3 ± 1.3***, ##
Insulin (ng/ml)	1.82 ± 0.23	1.57 ± 0.15	0.21 ± 0.09***	0.24 ± 0.1***	0.11 ± 0.07***	0.30 ± 0.10***
TAG (mg/dl)	80.6 ± 4.3	66.5 ± 6.2	83.6 ± 15.2	89.5 ± 12.2	56.0 ± 18.8	79.4 ± 19.3
NEFA (μeq/liter)	522.9 ± 45.7	469.6 ± 51.3	508.2 ± 72.0	525.8 ± 94.1	497.2 ± 106.4	702.8 ± 128.0
T-Cho (mg/dl)	63.7 ± 4.4	60.5 ± 3.0	73.1 ± 7.9	80.7 ± 7.0	85.8 ± 12.9	104.4 ± 9.7***, #
F-Cho (mg/dl)	20.8 ± 1.2	20.0 ± 0.7	25.1 ± 2.1	27.1 ± 1.8**	25.2 ± 2.6	31.0 ± 2.3***

[a] NEFA, nonesterified fatty acid; T-Cho, total cholesterol; F-Cho, free cholesterol.
[b] **, $P < 0.01$; ***, $P < 0.001$, against saline-treated mice of each genotype; #, $P < 0.05$; ##, $P < 0.01$, against STZ-treated mice of each genotype. For glucose, $n = 6$ to 10 per group; for insulin, $n = 9$ per group; for TAG and NEFA, $n = 9$ to 16 per group; for T- and F-Cho, $n = 5$ to 7 per group.

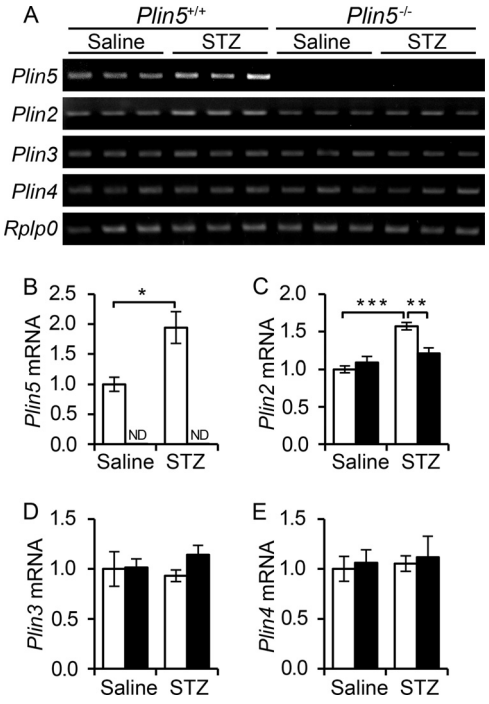

FIG 4 Expression of *Plin* and lipase mRNAs in the heart. Expression of each *Plin* mRNA was quantified by RT-PCR using total heart RNA. (A) Result of electrophoresis of the PCR products. mRNA expression of *Plin5* (B), *Plin2* (C), *Plin3* (D), and *Plin4* (E) relative to that in saline-treated control WT mice was estimated by densitometry of the electropherogram, using ImageJ software ($n = 3$ per group). The *Rplp0* gene was used as an internal control. Open bars, WT mice; filled bars, *Plin5*$^{-/-}$ mice; ND, not detectable. Data are shown as means ± SEM (*, $P < 0.05$; **, $P < 0.01$; ***, $P < 0.001$).

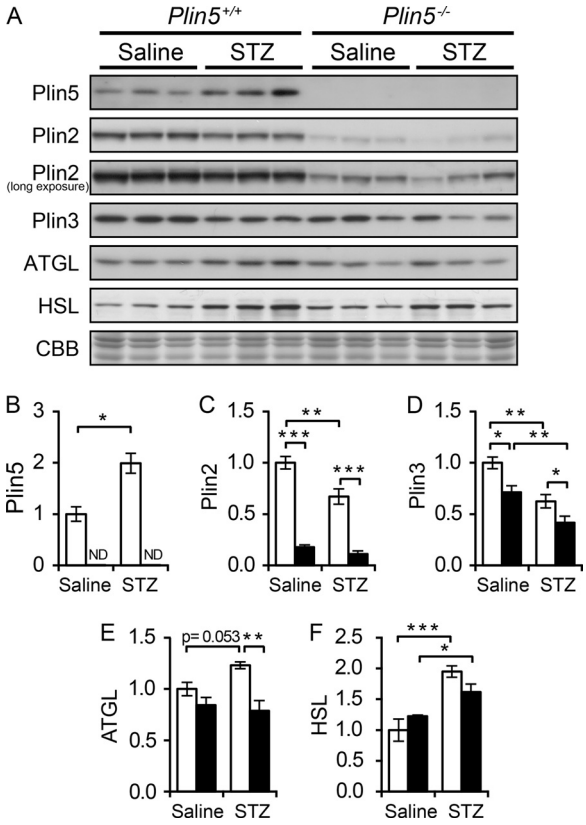

FIG 5 Levels of Plin and lipase proteins in the heart. (A) Images of immunoblotting of Plin proteins and lipases using total protein extracts from the heart (15 μg of total protein per lane). Coomassie brilliant blue (CBB) staining of the gel was used as a loading control. (B to F) The graphs show the levels of Plin5, Plin2, Plin3, ATGL, and HSL relative to those in saline-treated control WT mice ($n = 3$ per group). Open bars, WT mice; filled bars, *Plin5*$^{-/-}$ mice; ND, not detectable. Data are shown as means ± SEM (*, $P < 0.05$; **, $P < 0.01$; and ***, $P < 0.001$).

such minute LDs. We examined the intracellular location of these structures by immunofluorescence microscopy, employing an antibody to Plin2 (Fig. 2C, panels a and b). In agreement with our previous result (11), Plin2-positive signals were detected in the hearts of diabetic *Plin5*$^{-/-}$ mice although LDs were morphologically undetectable by electron microscopy. We further investigated their intramyocardial distribution by immunoelectron microscopy by using a Plin2-specific antibody, employing the preembedding technique to obtain clear images of the membranes (Fig. 2C, panels c and d). In the hearts of diabetic WT mice, Plin2 localized to the surface of LDs, which were buried between mitochondria. In the hearts of diabetic *Plin5*$^{-/-}$ mice, most but not all Plin2 signals were observed in proximity of mitochondria, though not between them. Thus, the Plin2-coated minute LDs are still located close to mitochondria but may not be adhering to them, despite the absence of Plin5. This result is not necessarily inconsistent with the notion that Plin5 is involved in the close contact of LDs with mitochondria (33, 34).

Expression of other Plin proteins and lipases in WT and *Plin5*$^{-/-}$ mice. The above observations indicate that Plin5 is essential to maintain LDs in the hearts of type 1 diabetic mice. Other Plin proteins expressed in the heart, that is, Plin2, Plin3, and Plin4, do not compensate for Plin5 under physiological conditions (11). Accordingly, we measured their heart mRNA and protein levels in WT and *Plin5*$^{-/-}$ mice in both control and diabetic states. The mRNA expression of *Plin2* increased in diabetic WT mice but did not change in *Plin5*$^{-/-}$ mice (Fig. 4A and C). *Plin3* and *Plin4* mRNAs were expressed at comparable levels in both genotypes under both conditions (Fig. 4A, D, and E). In WT mice, despite the increased or unchanged mRNA levels, the protein levels of Plin2 and Plin3 were lower in the hearts of diabetic mice than in those of nondiabetic control mice (Fig. 5A, C, and D). In *Plin5*$^{-/-}$ mice, the Plin2 protein level decreased markedly whereas Plin3 decreased moderately under both nondiabetic and diabetic conditions. The decrease in Plin2 protein is similar to that observed for *Plin5*$^{-/-}$ mice in the normal physiological state (11), representing the degradation of unbound Plin2 protein by proteasomes. These results indicate that other Plin proteins do not compensate for the deficiency of Plin5 in the aberrant lipid accumulation during type 1 diabetes.

We also measured the protein levels of the major heart lipases, ATGL and HSL. Levels of both lipases increased in the hearts of diabetic WT mice; however, in diabetic *Plin5*$^{-/-}$ mice, ATGL did not increase, and HSL increased to a lesser extent than in WT mice (Fig. 5E and F).

***Plin5*$^{-/-}$ mice are resistant to diabetes-induced heart malfunction due to lower oxidative stress.** It has been reported that intramyocardial aberrant lipid accumulation affects heart function (2, 3). Because diabetic *Plin5*$^{-/-}$ mice lacked LDs in the heart, we expected that the heart function of diabetic *Plin5*$^{-/-}$ mice

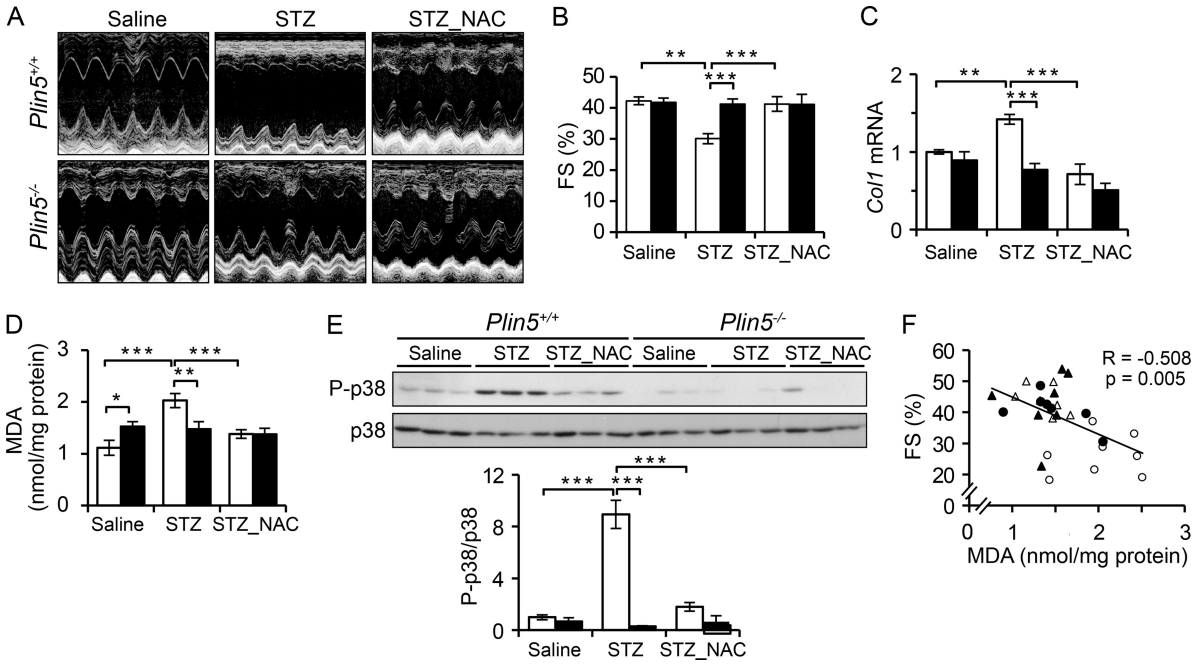

FIG 6 Diabetes-induced heart malfunction is suppressed by *Plin5* deficiency. (A) Representative images of echocardiography (M mode) of nondiabetic, diabetic, and NAC-treated diabetic mice (WT and *Plin5*$^{-/-}$), at heart rates of ca. 450 beats per min. (B) FS ($n = 10$ to 19 per group) calculated from the echocardiographs. (C) Heart expression of *ColI* mRNA, a marker of heart fibrosis, relative to that of saline-treated control WT mice, normalized with the signal intensity of *Rplp0* ($n = 4$ per group). (D) Amount of MDA, a marker of oxidative stress, measured by the TBARS assay ($n = 7$ to 10 per group). (E) Immunoblotting of phosphorylated and total p38 (P-p38 and p38, respectively), using total heart protein extracts. The graph shows the ratio of P-p38 to total p38, relative to that of saline-treated control WT mice ($n = 3$ per group). For panels B to E, data are shown as means ± SEM (**, $P < 0.01$; ***, $P < 0.001$). Open bars, WT mice; filled bars, *Plin5*$^{-/-}$ mice. (F) Regression analysis of the correlation between the heart MDA content and FS. Open circles, diabetic WT mice; open triangles, NAC-treated diabetic WT mice; filled circles, diabetic *Plin5*$^{-/-}$ mice; filled triangles, NAC-treated diabetic *Plin5*$^{-/-}$ mice.

would not be affected. To examine this notion, we assessed heart function by echocardiography (Fig. 6A and B). FS, a representative of heart function, decreased significantly in diabetic WT mice compared with values in nondiabetic WT mice. In contrast, the FS values in diabetic *Plin5*$^{-/-}$ mice were indistinguishable from the values in nondiabetic WT and *Plin5*$^{-/-}$ mice. We also measured the type 1 collagen (*ColI*) mRNA level, a marker of fibrosis, in the heart. In diabetic WT mice but not in *Plin5*$^{-/-}$ mice, the mRNA level increased (Fig. 6C). On the other hand, body weight, heart weight, and the levels of blood glucose and insulin were comparable between diabetic WT and *Plin5*$^{-/-}$ mice (Table 2). Thus, *Plin5*$^{-/-}$ mice can serve as a type 1 diabetes cardiomyopathy-resistant model though the diabetic state is the same as that of WT mice.

To understand the mechanism describing how aberrant lipid accumulation induces heart malfunction, we further analyzed the metabolic parameters of type 1 diabetic *Plin5*$^{-/-}$ mice in comparison with those of diabetic WT mice. Several previous studies suggested that elevation of oxidative stress in the diabetic heart is a factor contributing to the development and progression of diabetic cardiomyopathy (17, 26, 35). Therefore, we examined whether the diabetes-induced increase in oxidative stress is suppressed by *Plin5* deficiency by measuring MDA, a derivative of lipid peroxide (Fig. 6D). MDA content in the hearts of diabetic WT mice was 2-fold higher than in nondiabetic WT mice. In contrast, MDA contents were indistinguishable between nondiabetic and diabetic *Plin5*$^{-/-}$ mice; the MDA value was higher than that of WT mice in the nondiabetic state, as described previously (11), but lower than that of WT mice under the diabetic conditions. Next, we measured the phosphorylation level of p38 mitogen-activated protein kinase, a mediator and a marker of oxidative stress. The ratio of phosphorylated p38 to total p38 was enhanced in diabetic WT mice but not in *Plin5*$^{-/-}$ mice (Fig. 6E). To confirm that the diabetes-induced heart malfunction of WT mice was due to increased ROS production, we administered an antioxidant, NAC, to the mice. Long-term NAC treatment suppressed the diabetes-induced escalation of heart malfunction (Fig. 6B), cardiac fibrosis (Fig. 6C), oxidative stress (Fig. 6D), and p38 phosphorylation (Fig. 6E). Significantly, the heart MDA level inversely correlated with FS (Fig. 6F). These results indicate that elevated ROS generation is a major cause of diabetes-induced heart malfunction in WT mice. In contrast, *Plin5*$^{-/-}$ mice are protected from the decline in heart function by mitigated ROS generation in the diabetic state.

Expression levels of PPARα target genes and mitochondrial capacities for ROS production are similar between the two genotypes. It has been reported that the PPARα regulatory pathway is activated in the hearts of diabetic mice, which results in imbalances of myocardial energy metabolism, leading to diabetic cardiomyopathy (16, 17). It has also been reported that LDs are the source of lipid ligands for PPARα activation, supplying FAs through hydrolysis of TAG (36–38). In the hearts of type 1-diabetic *Plin5*$^{-/-}$ mice, LDs were undetectable, a result which might affect the supply of lipid ligands to PPARα. Accordingly, by immunoblotting, we measured the protein levels of PPARα target genes, *Acox*, *UCP3*, *VLCAD*, and *MCAD* (Fig. 7A). Protein levels

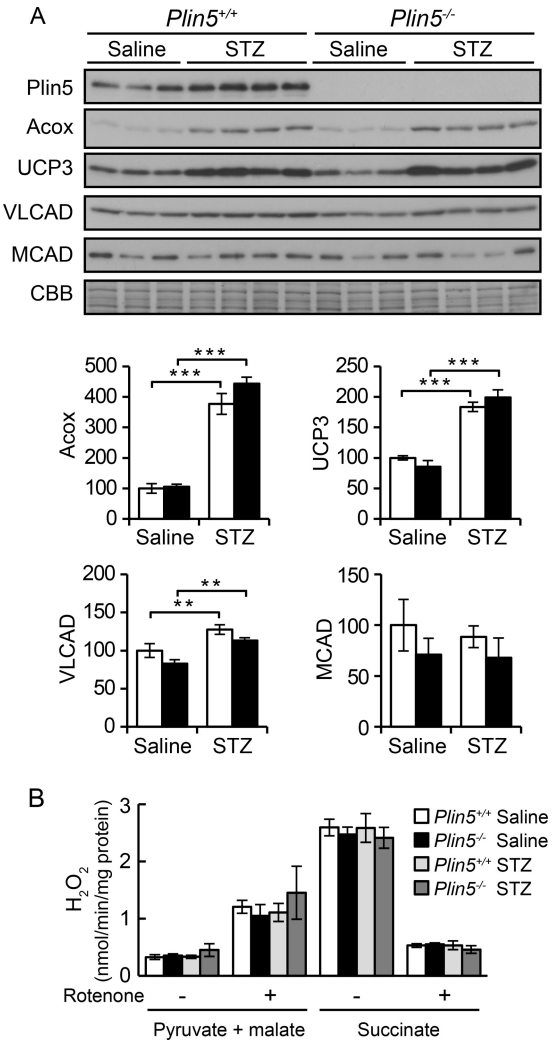

FIG 7 Levels of proteins encoded by PPARα target genes and mitochondrial ROS generation capacities are not different between the genotypes. (A) Protein levels of PPARα target genes, Plin5, Acox, UCP3, LCAD, and MCAD, in the hearts of nondiabetic and diabetic WT (open bars) and *Plin5*$^{-/-}$ (filled bars) mice. The lower graphs show amounts of each protein relative to amounts in saline-treated control WT mice. Coomassie brilliant blue (CBB) staining of the gel was used as a loading control. (B) Evaluation of mitochondrial ROS generation capacity estimated by hydrogen peroxide production with isolated mitochondria from nondiabetic and diabetic WT and *Plin5*$^{-/-}$ mice ($n = 5$ to 9 per group). Data are shown as means ± SEM (**, $P < 0.01$; ***, $P < 0.001$).

of Acox, UCP3, and VLCAD were upregulated by diabetes in the hearts of both genotypes of mice. On the other hand, the MCAD level in diabetic mice was comparable to that of nondiabetic mice of either genotype.

Several previous papers reported that the mitochondrial electron transport chain is one of the major sites of ROS generation in the diabetic heart, contributing to heart malfunction (25–27, 35). In contrast, other reports show that progression of diabetes does not affect the capacity of ROS generation by mitochondria (39, 40). Using isolated mitochondria, we examined whether the lower ROS production in the hearts of type 1-diabetic *Plin5*$^{-/-}$ mice was due to a lower capacity than WT mice for mitochondrial ROS generation (Fig. 7B). Superoxide production, by electron leak during forward electron transport through complexes 1 and 3, was assessed by the rate of H_2O_2 production with pyruvate and malate as substrates. The results did not differ among the four mouse groups. With the addition of rotenone, a specific inhibitor of complex 1, the rate of H_2O_2 production increased due to reverse electron transport, and the rates were similar among the four groups. With succinate as the substrate of complex 2, superoxide production, due to reverse electron transport to complex 1 and forward transport to complex 3, was measured and also did not differ among the four groups. With the addition of rotenone, the rate of H_2O_2 production decreased due to blocking of the reverse electron transport, and the rates were indistinguishable among the four groups. These results suggest that suppression of type 1 diabetes-induced heart malfunction in *Plin5*$^{-/-}$ mice is not caused by repression of the PPARα transcriptional regulatory pathway nor by a lower capacity for mitochondrial ROS generation.

Accumulation of lipotoxic molecules and activation of NADPH oxidase are suppressed in the hearts of *Plin5*$^{-/-}$ mice. FA, DAG, and ceramide are signaling lipids, and an increase of intramyocardial levels is considered toxic. In fact, several papers report that increased levels of lipotoxic molecules lead to heart malfunction (41, 42). Expecting that the intramyocardial levels of such molecules, similar to TAG, would be lower in *Plin5*$^{-/-}$ mice than in WT mice in the type 1-diabetic state, we measured intramyocardial levels of these molecules (Fig. 8). In diabetic WT mice, accumulation of FA, *sn*-1,2-DAG, and ceramide was observed. In contrast, these molecules did not accumulate above the control levels in the hearts of diabetic *Plin5*$^{-/-}$ mice. Interestingly, *sn*-1,2-DAG and ceramide, but not TAG and FA (Fig. 2B and 8A), decreased in the hearts of NAC-treated diabetic WT mice compared with levels in untreated diabetic WT mice. Plasma TAG and FA concentrations were not affected by NAC treatment although total and free cholesterol levels were higher in NAC-treated diabetic *Plin5*$^{-/-}$ mice (Table 2).

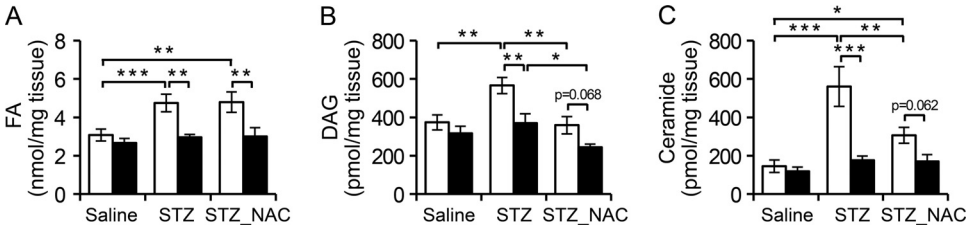

FIG 8 Accumulation of lipotoxic molecules is suppressed in the hearts of *Plin5*$^{-/-}$ mice. Levels of FA (A), *sn*-1,2-DAG (B), and ceramide (C) in the hearts of nondiabetic and diabetic WT and *Plin5*$^{-/-}$ mice ($n = 5$ to 8 per group). FA was measured by a colorimetric method, whereas DAG and ceramide were measured by the DAG kinase method. Open bars, WT mice; filled bars, *Plin5*$^{-/-}$ mice. Data are shown as means ± SEM (*, $P < 0.05$; **, $P < 0.01$; ***, $P < 0.001$).

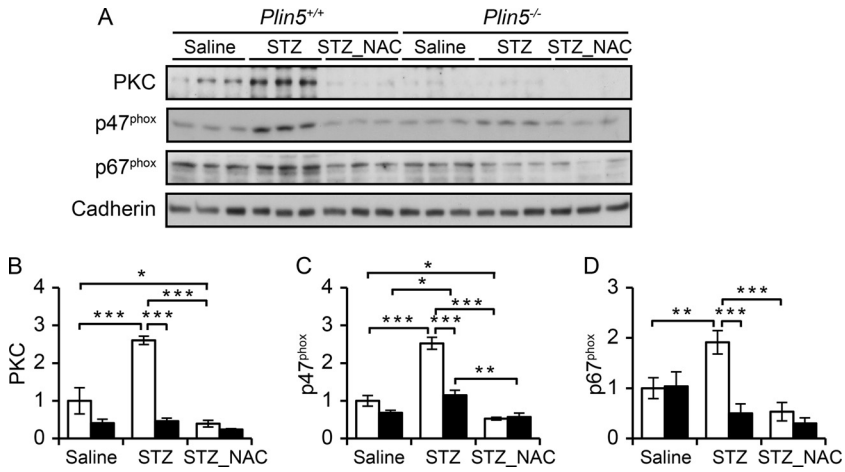

FIG 9 Translocation of PKC, p47^{phox}, and p67^{phox} to the plasma membrane is suppressed in the hearts of *Plin5*$^{-/-}$ mice. (A) Images of immunoblotting for PKC, p47^{phox}, and p67^{phox} using the heart membrane fractions prepared from WT and *Plin5*$^{-/-}$ mice. Cadherin was used as a loading control. Amounts of membranous PKC (B), p47^{phox} (C), and p67^{phox} (D) relative to those in saline-treated control WT mice were estimated using ImageJ software ($n = 3$ per group). Open bars, WT mice; filled bars, *Plin5*$^{-/-}$ mice. Data are shown as means ± SEM (*, $P < 0.05$; **, $P < 0.01$; ***, $P < 0.001$).

Several reports show that NADPH oxidase 2 (NOX2) is another major source of ROS generation (43–45). The NOX2 enzyme complex consists of membrane-bound subunits (NOX2/gp91 and p22) and cytosolic subunits (p47^{phox}, p67^{phox}, p40^{phox}, and Rac) (46). Upon phosphorylation of p47^{phox} by PKC, these subunits are assembled on the plasma membrane and hence the enzyme is activated. DAG and ceramide activate PKC by recruiting the enzyme to the membrane (47, 48). Hence, we expected that the levels of active PKC and the NOX2 enzyme complex in the membrane would increase in the hearts of type 1-diabetic WT mice but not in *Plin5*$^{-/-}$ mice due to the increased levels of lipotoxic molecules. To examine this supposition, we estimated the membranous protein levels of PKC (mainly corresponding to α and β2 isoforms, based on the electrophoretic mobility and published data on heart expression [49]), p47^{phox}, and p67^{phox} by immunoblotting membrane fractions (Fig. 9). In the hearts of diabetic WT mice but not in *Plin5*$^{-/-}$ mice, membranous levels of PKC, p47^{phox}, and p67^{phox} were higher than those of the nondiabetic mice. In agreement with previous studies (50–52), membranous levels of PKC, p47^{phox}, and p67^{phox} decreased in the hearts of antioxidant-treated diabetic mice compared with levels in diabetic mice of both genotypes. Taken together, these results suggest that suppression of STZ-induced type 1 diabetic heart malfunction in *Plin5*$^{-/-}$ mice is due to suppression of NOX activation through the DAG/ceramide-PKC pathway.

DISCUSSION

We previously reported that Plin5 protects heart LDs from attack by ATGL and/or a related lipase(s) *in vivo* under physiological conditions (11). In this study, we demonstrated that *Plin5*$^{-/-}$ mice, also in the STZ-induced type 1 diabetic state, lack detectable LDs in the heart and consequently do not exhibit diabetes-induced aberrant lipid accumulation in this organ. Intramyocardial aberrant TAG accumulation, typically observed in diabetes, is known to affect heart function in both humans and rodent models (2, 12). Type 1 diabetic *Plin5*$^{-/-}$ mice did not exhibit heart malfunction. Thus, Plin5 promotes aberrant TAG accumulation in the heart, affecting the organ function in type 1 diabetes, in contrast to the cardioprotective function under physiological conditions.

Plin5$^{-/-}$ mice could be a useful model with tolerance to type 1 diabetic cardiomyopathy, which would be helpful to study the disease mechanism by comparing metabolic parameters with those of WT mice. Levels of lipid intermediates, *sn*-1,2-DAG, ceramide, and FA, increased in the hearts of diabetic WT mice but not in *Plin5*$^{-/-}$ mice. Accumulation of these compounds, particularly DAG, has been noted in the hearts of STZ-induced diabetic animals (49, 53, 54) although the DAG isoform was unspecified in the majority of works. On the other hand, heart-specific overexpression of ATGL (55) and HSL (56) decreases those compounds and improves heart function in type 1 diabetes. Such compounds, but not TAG itself, are the likely causes of lipotoxicity, which has typically been shown by studies analyzing mice overexpressing the heart-specific DAG acyltransferase 1 (DGAT1) (28, 29). These mice exhibited TAG accumulation as well as decreases in FA, DAG, and ceramide in the heart concomitantly with improved heart function in genetic background of lipotoxic heart malfunction (that is, cardiac fatty acyl-CoA synthase [28] and PPARγ [29] overexpression).

DAG, more specifically *sn*-1,2-DAG, is a known activator of conventional and novel PKC isoforms (57), whereas ceramide activates an atypical PKC (48). In the present work, we observed PKC translocation to membranes, which is an indicator of enzyme activation, in STZ-induced diabetic WT mice but not *Plin5*$^{-/-}$ mice. Heart PKC activation was previously shown in type 1 diabetic mice (49, 50, 52), and a PKC inhibitor ameliorated STZ-induced cardiac dysfunction (52) as well as vascular dysfunction (58). Moreover, heart-specific PKCβ2 overexpression causes cardiomyopathy (59). Hence, PKC activation by DAG has been implicated in heart complications due to type 1 diabetes (54). In line with this notion, STZ-induced cardiomyopathy was alleviated by islet transplantation, with concomitant reduction of heart DAG level and PKC activity (49). A study in DGAT1 transgenic mice also showed a concomitant decrease in lipotoxic compounds and PKC activity (29). Our present results further show that, by Plin5 ablation, lower contents of lipotoxic compounds and lower PKC activity together are associated with normal heart function in type

1 diabetes. It should also be noted, however, that DAG may exert signaling functions through non-PKC receptors (60).

Excess ROS production has been implicated in diabetes-induced heart malfunction. In the present study, heart ROS production increased in diabetic WT mice but not in *Plin5*$^{-/-}$ mice. Moreover, long-term treatment of WT mice with an antioxidant reduced the diabetes-induced oxidative stress, as assessed by MDA content and p38 phosphorylation level, and impairment of heart function was prevented without alteration of TAG or FA levels. These results indicate that aberrant LD formation and TAG accumulation lead to type 1 diabetes-induced heart malfunction, primarily through excess ROS generation.

It was reported that, under diabetic conditions, heart expression of PPARα target genes increases and that FA oxidation accelerates, resulting in excess mitochondrial ROS generation (16, 17, 25–27, 61). It was also reported that LDs supply lipid ligands, FAs and their metabolites, for PPARα activation through lipolysis (22, 36–38). In the hearts of diabetic *Plin5*$^{-/-}$ mice, LDs were not detectable, and the intramyocardial FA levels were lower than those of diabetic WT mice. Nevertheless, the protein levels of PPARα target genes and mitochondrial ROS generation capacities were indistinguishable between the two genotypes under either normal or diabetic conditions. Despite the lower heart FA contents in *Plin5*$^{-/-}$ mice due to facilitated mitochondrial oxidation (11), a sufficient amount of lipids is likely to be supplied to activate PPARα. Taking these results together, at least under our experimental conditions of STZ-induced type 1 diabetes, abnormal PPARα activation and/or mitochondrial ROS production do not seem to be major causes of heart malfunction. Although mitochondria are major sites of ROS generation in the heart and are implicated in cardiomyopathy caused by both type 1 and type 2 diabetes, cytoplasmic ROS production, including by NOX, has also drawn attention (61). Mitochondrial dysfunction is often observed in the hearts of diabetic animals and can be either the cause or result of oxidative stress. Moreover, mitochondrial and cytoplasmic ROS may affect the functions, including ROS generation itself, of reciprocal compartments. It is possible that the primary origin of ROS varies depending on experimental conditions, such as diabetes-inducing procedures, durations of treatments, and severity of diabetic state.

Membranous levels of NOX subunits, p47^{phox} and p67^{phox}, were elevated in diabetic WT mice but not *Plin5*$^{-/-}$ mice. Activated PKC causes activation of NOX2 through phosphorylation of p47^{phox} (47, 48, 62). A study employing a PKCβ2 inhibitor showed decreased NOX2 activity and ROS level, together with the improvement of heart function (52). The importance of NOX2 in STZ-induced ROS production and heart impairment was shown by the ameliorating effects of a NOX2 inhibitor, apocynin, on heart parameters (45, 51). In addition, Rac1 ablated mice, in which the assembly of NOX2 complex on plasma membrane is suppressed, are tolerant to type 1 diabetes-induced cardiac malfunction (44). Treatment of animals with an antioxidant, NAC, was shown to correct heart abnormalities induced by type 1 diabetes (50, 51). It is of interest that these compounds simultaneously result in reduced activation of PKC and NADPH oxidase. We found that NAC reduced DAG and ceramide but not FA and diminished PKC and NOX2 activation. A similar effect of decreasing DAG was observed with α-tocopherol in the aorta (63) and mesangial cells (64). This was proposed to be due to protection of DAG kinase from oxidative stress, thereby directing DAG to phospholipid synthesis. Thus, ROS may in turn activate PKC by enhancing DAG accumulation.

The results of preceding studies together suggest the involvement of PKC activation by DAG and/or ceramide, leading to excess ROS generation, in type 1 diabetes-induced cardiomyopathy. However, to the best of our knowledge, no study thus far has presented consistent alterations of the consecutive parameters in the whole signaling pathway in any experimental settings. By ablating Plin5, a key regulator of TAG metabolism, we successfully showed the correction of all the downstream parameters in STZ-induced diabetes, conceivably placing the alteration in lipid metabolism farthest upstream. *Plin5*$^{-/-}$ mice are resistant to type 1 diabetes-induced heart malfunction owing to decreased oxidative stress, despite the age-dependent heart malfunction due to enhanced mitochondrial ROS generation, under physiological conditions (11). It is likely that heart FA oxidation and ROS production in mitochondria would increase in *Plin5*$^{-/-}$ mice compared with levels in WT mice in both physiological and diabetic states. Thus, ROS production by NOX2 in the hearts of diabetic WT mice would far exceed ROS generation in mitochondria in *Plin5*$^{-/-}$ mice.

Taking these results together, we suggest that Plin5 allows excess TAG accumulation in the hearts of mice with STZ-induced type 1 diabetes, which is accompanied by an increase of lipotoxic compounds, such as DAG and ceramide. These compounds lead to activation of NOX2 via the PKC signaling pathway, resulting in excess ROS production and eventual diabetic cardiomyopathy. With the positive feedback loop leading to DAG increase, ROS would promote heart impairment by promoting diverse PKC signaling pathways as well as direct oxidative toxicity. A trial to temporarily suppress Plin5 function would potentially be beneficial for ameliorating cardiomyopathy, during which diabetes itself may be treated effectively by an appropriate means. Long-term suppression of Plin5 function, however, would accelerate heart malfunction, as suggested by our previous observations (11). The effect of Plin5 ablation on cardiomyopathy should also be evaluated in other experimental diabetes models.

ACKNOWLEDGMENTS

This work was supported in part by a grant from the Japan Society for the Promotion of Science (JSPS KAKENHI; grant 25440053) to T.O. and by a grant from the Naito Foundation to K.K.

REFERENCES

1. **Lopaschuk GD, Ussher JR, Folmes CDL, Jaswal JS, Stanley WC.** 2010. Myocardial fatty acid metabolism in health and disease. Physiol. Rev. **90:** 207–258. http://dx.doi.org/10.1152/physrev.00015.2009.
2. **Bugger H, Abel ED.** 2009. Rodent models of diabetic cardiomyopathy. Dis. Model. Mech. **2:**454–466. http://dx.doi.org/10.1242/dmm.001941.
3. **Goldberg IJ, Trent CM, Schulze PC.** 2012. Lipid metabolism and toxicity in the heart. Cell Metab. **15:**805–812. http://dx.doi.org/10.1016/j.cmet.2012.04.006.
4. **Farese RV, Walther TC.** 2009. Lipid droplets finally get a little R-E-S-P-E-C-T. Cell **139:**855–860. http://dx.doi.org/10.1016/j.cell.2009.11.005.
5. **Reue K.** 2011. A thematic review series: lipid droplet storage and metabolism: from yeast to man. J. Lipid Res. **52:**1865–1868. http://dx.doi.org/10.1194/jlr.E020602.
6. **Kimmel AR, Brasaemle DL, McAndrews-Hill M, Sztalryd C, Londos C.** 2010. Adoption of Perilipin as a unifying nomenclature for the mammalian PAT-family of intracellular lipid storage droplet proteins. J. Lipid Res. **51:**468–471. http://dx.doi.org/10.1194/jlr.R000034.
7. **Bickel PE, Tansey JT, Welte MA.** 2009. PAT proteins, an ancient family of lipid droplet proteins that regulate cellular lipid stores. Biochim. Biophys. Acta **1791:**419–440. http://dx.doi.org/10.1016/j.bbalip.2009.04.002.

8. **Yamaguchi T, Matsushita S, Motojima K, Hirose F, Osumi T.** 2006. MLDP, a novel PAT family protein localized to lipid droplets and enriched in the heart, is regulated by peroxisome proliferator-activated receptor α. J. Biol. Chem. **281:**14232–14240. http://dx.doi.org/10.1074/jbc.M601682200.
9. **Wolins NE, Quaynor BK, Skinner JR, Tzekov A, Croce MA, Gropler MC, Varma V, Yao-Borengasser A, Rasouli N, Kern PA, Finck BN, Bickel PE.** 2006. OXPAT/PAT-1 is a PPAR-induced lipid droplet protein that promotes fatty acid utilization. Diabetes **55:**3418–3428. http://dx.doi.org/10.2337/db06-0399.
10. **Dalen KT, Dahl T, Holter E, Arntsen B, Londos C, Sztalryd C, Nebb HI.** 2007. LSDP5 is a PAT protein specifically expressed in fatty acid oxidizing tissues. Biochim. Biophys. Acta **1771:**210–227. http://dx.doi.org/10.1016/j.bbalip.2006.11.011.
11. **Kuramoto K, Okamura T, Yamaguchi T, Nakamura TY, Wakabayashi S, Morinaga H, Nomura M, Yanase T, Otsu K, Usuda N, Matsumura S, Inoue K, Fushiki T, Kojima Y, Hashimoto T, Sakai F, Hirose F, Osumi T.** 2012. Perilipin 5, a lipid droplet-binding protein, protects heart from oxidative burden by sequestering fatty acid from excessive oxidation. J. Biol. Chem. **287:**23852–23863. http://dx.doi.org/10.1074/jbc.M111.328708.
12. **Rijzewijk LJ, van der Meer RW, Smit JW, Diamant M, Bax JJ, Hammer S, Romijn JA, de Roos A, Lamb HJ.** 2008. Myocardial steatosis is an independent predictor of diastolic dysfunction in type 2 diabetes mellitus. J. Am. Coll. Cardiol. **52:**1793–1799. http://dx.doi.org/10.1016/j.jacc.2008.07.062.
13. **Poornima IG, Parikh P, Shannon RP.** 2006. Diabetic cardiomyopathy: the search for a unifying hypothesis. Circ. Res. **98:**596–605. http://dx.doi.org/10.1161/01.RES.0000207406.94146.c2.
14. **Regan TJ, Lyons MM, Ahmed SS, Levinson GE, Oldewurtel HA, Ahmad MR, Haider B.** 1977. Evidence for cardiomyopathy in familial diabetes mellitus. J. Clin. Invest. **60:**884–899.
15. **McGavock JM, Lingvay I, Zib I, Tillery T, Salas N, Unger R, Levine BD, Raskin P, Victor RG, Szczepaniak LS.** 2007. Cardiac steatosis in diabetes mellitus: a ^{1}H-magnetic resonance spectroscopy study. Circulation **116:**1170–1175. http://dx.doi.org/10.1161/CIRCULATIONAHA.106.645614.
16. **Finck BN, Lehman JJ, Leone TC, Welch MJ, Bennett MJ, Kovacs A, Han X, Gross RW, Kozak R, Lopaschuk GD, Kelly DP.** 2002. The cardiac phenotype induced by PPARα overexpression mimics that caused by diabetes mellitus. J. Clin. Invest. **109:**121–130. http://dx.doi.org/10.1172/JCI14080.
17. **Finck BN, Han X, Courtois M, Aimond F, Nerbonne JM, Kovacs A, Gross RW, Kelly DP.** 2003. A critical role for PPARα-mediated lipotoxicity in the pathogenesis of diabetic cardiomyopathy: modulation by dietary fat content. Proc. Natl. Acad. Sci. U. S. A. **100:**1226–1231. http://dx.doi.org/10.1073/pnas.0336724100.
18. **Son N-H, Yu S, Tuinei J, Arai K, Hamai H, Homma S, Shulman GI, Abel ED, Goldberg IJ.** 2010. PPARγ-induced cardiolipotoxicity in mice is ameliorated by PPARα deficiency despite increases in fatty acid oxidation. J. Clin. Invest. **120:**3443–3454. http://dx.doi.org/10.1172/JCI40905.
19. **Chiu HC, Kovacs A, Ford DA, Hsu FF, Garcia R, Herrero P, Saffitz JE, Schaffer JE.** 2001. A novel mouse model of lipotoxic cardiomyopathy. J. Clin. Invest. **107:**813–822. http://dx.doi.org/10.1172/JCI10947.
20. **Ellis JM, Mentock SM, Depetrillo MA, Koves TR, Sen S, Watkins SM, Muoio DM, Cline GW, Taegtmeyer H, Shulman GI, Willis MS, Coleman RA.** 2011. Mouse cardiac acyl coenzyme a synthetase 1 deficiency impairs fatty acid oxidation and induces cardiac hypertrophy. Mol. Cell. Biol. **31:**1252–1262. http://dx.doi.org/10.1128/MCB.01085-10.
21. **Kienesberger PC, Pulinilkunnil T, Sung MM, Nagendran J, Haemmerle G, Kershaw EE, Young ME, Light PE, Oudit GY, Zechner R, Dyck JRB.** 2012. Myocardial ATGL overexpression decreases the reliance on fatty acid oxidation and protects against pressure overload-induced cardiac dysfunction. Mol. Cell. Biol. **32:**740–750. http://dx.doi.org/10.1128/MCB.06470-11.
22. **Zierler KA, Jaeger D, Pollak NM, Eder S, Rechberger GN, Radner FPW, Woelkart G, Kolb D, Schmidt A, Kumari M, Preiss-Landl K, Pieske B, Mayer B, Zimmermann R, Lass A, Zechner R, Haemmerle G.** 2013. Functional cardiac lipolysis in mice critically depends on comparative gene identification-58. J. Biol. Chem. **288:**9892–9904. http://dx.doi.org/10.1074/jbc.M112.420620.
23. **Pollak NM, Schweiger M, Jaeger D, Kolb D, Kumari M, Schreiber R, Kolleritsch S, Markolin P, Grabner GF, Heier C, Zierler KA, Rülicke T, Zimmermann R, Lass A, Zechner R, Haemmerle G.** 2013. Cardiac-specific overexpression of perilipin 5 provokes severe cardiac steatosis via the formation of a lipolytic barrier. J. Lipid Res. **54:**1092–1102. http://dx.doi.org/10.1194/jlr.M034710.
24. **Wang H, Sreenivasan U, Gong D-W, O'Connell KA, Dabkowski ER, Hecker PA, Ionica N, Konig M, Mahurkar A, Sun Y, Stanley WC, Sztalryd C.** 2013. Cardiomyocyte-specific perilipin 5 overexpression leads to myocardial steatosis and modest cardiac dysfunction. J. Lipid Res. **54:**953–965. http://dx.doi.org/10.1194/jlr.M032466.
25. **Shen X, Zheng S, Metreveli NS, Epstein PN.** 2006. Protection of cardiac mitochondria by overexpression of MnSOD reduces diabetic cardiomyopathy. Diabetes **55:**798–805. http://dx.doi.org/10.2337/diabetes.55.03.06.db05-1039.
26. **Boudina S, Sena S, Theobald H, Sheng X, Wright JJ, Hu XX, Aziz S, Johnson JI, Bugger H, Zaha VG, Abel ED.** 2007. Mitochondrial energetics in the heart in obesity-related diabetes: direct evidence for increased uncoupled respiration and activation of uncoupling proteins. Diabetes **56:**2457–2466. http://dx.doi.org/10.2337/db07-0481.
27. **Bugger H, Abel ED.** 2010. Mitochondria in the diabetic heart. Cardiovasc. Res. **88:**229–240. http://dx.doi.org/10.1093/cvr/cvq239.
28. **Liu L, Shi X, Bharadwaj KG, Ikeda S, Yamashita H, Yagyu H, Schaffer JE, Yu Y-H, Goldberg IJ.** 2009. DGAT1 expression increases heart triglyceride content but ameliorates lipotoxicity. J. Biol. Chem. **284:**36312–36323. http://dx.doi.org/10.1074/jbc.M109.049817.
29. **Liu L, Yu S, Khan RS, Homma S, Schulze PC, Blaner WS, Yin Y, Goldberg IJ.** 2012. Diacylglycerol acyl transferase 1 overexpression detoxifies cardiac lipids in PPARγ transgenic mice. J. Lipid Res. **53:**1482–1492. http://dx.doi.org/10.1194/jlr.M024208.
30. **Hashiguchi N, Kojidani T, Imanaka T, Haraguchi T, Hiraoka Y, Baumgart E, Yokota S, Tsukamoto T, Osumi T.** 2002. Peroxisomes are formed from complex membrane structures in PEX6-deficient CHO cells upon genetic complementation. Mol. Biol. Cell **13:**711–722. http://dx.doi.org/10.1091/mbc.01-10-0479.
31. **Shimabukuro M, Zhou YT, Levi M, Unger RH.** 1998. Fatty acid-induced beta cell apoptosis: a link between obesity and diabetes. Proc. Natl. Acad. Sci. U. S. A. **95:**2498–2502. http://dx.doi.org/10.1073/pnas.95.5.2498.
32. **Barja G.** 2002. The quantitative measurement of H_2O_2 generation in isolated mitochondria. J. Bioenerg. Biomembr. **34:**227–233. http://dx.doi.org/10.1023/A:1016039604958.
33. **Wang H, Sreenivasan U, Sreenevasan U, Hu H, Saladino A, Polster BM, Lund LM, Gong D-w, Stanley WC, Sztalryd C.** 2011. Perilipin 5, a lipid droplet-associated protein, provides physical and metabolic linkage to mitochondria. J. Lipid Res. **52:**2159–2168. http://dx.doi.org/10.1194/jlr.M017939.
34. **Bosma M, Minnaard R, Sparks LM, Schaart G, Losen M, de Baets MH, Duimel H, Kersten S, Bickel PE, Schrauwen P, Hesselink MK.** 2012. The lipid droplet coat protein perilipin 5 also localizes to muscle mitochondria. Histochem. Cell Biol. **137:**205–216. http://dx.doi.org/10.1007/s00418-011-0888-x.
35. **Nakamura H, Matoba S, Iwai-Kanai E, Kimata M, Hoshino A, Nakaoka M, Katamura M, Okawa Y, Ariyoshi M, Mita Y, Ikeda K, Okigaki M, Adachi S, Tanaka H, Takamatsu T, Matsubara H.** 2012. p53 promotes cardiac dysfunction in diabetic mellitus caused by excessive mitochondrial respiration-mediated reactive oxygen species generation and lipid accumulation. Circ. Heart Fail. **5:**106–115. http://dx.doi.org/10.1161/CIRCHEARTFAILURE.111.961565.
36. **Haemmerle G, Moustafa T, Woelkart G, Büttner S, Schmidt A, van de Weijer T, Hesselink M, Jaeger D, Kienesberger PC, Zierler K, Schreiber R, Eichmann T, Kolb D, Kotzbeck P, Schweiger M, Kumari M, Eder S, Schoiswohl G, Wongsiriroj N, Pollak NM, Radner FPW, Preiss-Landl K, Kolbe T, Rülicke T, Pieske B, Trauner M, Lass A, Zimmermann R, Hoefler G, Cinti S, Kershaw EE, Schrauwen P, Madeo F, Mayer B, Zechner R.** 2011. ATGL-mediated fat catabolism regulates cardiac mitochondrial function via PPAR-α and PGC-1. Nat. Med. **17:**1076–1085. http://dx.doi.org/10.1038/nm.2439.
37. **Mottillo EP, Bloch AE, Leff T, Granneman JG.** 2012. Lipolytic products activate peroxisome proliferator-activated receptor (PPAR) α and δ in brown adipocytes to match fatty acid oxidation with supply. J. Biol. Chem. **287:**25038–25048. http://dx.doi.org/10.1074/jbc.M112.374041.
38. **Zechner R, Zimmermann R, Eichmann TO, Kohlwein SD, Haemmerle G, Lass A, Madeo F.** 2012. Fat signals—lipases and lipolysis in lipid metabolism and signaling. Cell Metab. **15:**279–291. http://dx.doi.org/10.1016/j.cmet.2011.12.018.
39. **Herlein JA, Fink BD, O'Malley Y, Sivitz WI.** 2009. Superoxide and

respiratory coupling in mitochondria of insulin-deficient diabetic rats. Endocrinology **150:**46–55. http://dx.doi.org/10.1210/en.2008-0404.
40. **Bugger H, Boudina S, Hu XX, Tuinei J, Zaha VG, Theobald HA, Yun UJ, McQueen AP, Wayment B, Litwin SE, Abel ED.** 2008. Type 1 diabetic akita mouse hearts are insulin sensitive but manifest structurally abnormal mitochondria that remain coupled despite increased uncoupling protein 3. Diabetes **57:**2924–2932. http://dx.doi.org/10.2337/db08-0079.
41. **van de Weijer T, Schrauwen-Hinderling VB, Schrauwen P.** 2011. Lipotoxicity in type 2 diabetic cardiomyopathy. Cardiovasc. Res. **92:**10–18. http://dx.doi.org/10.1093/cvr/cvr212.
42. **Park T-S, Hu Y, Noh H-L, Drosatos K, Okajima K, Buchanan J, Tuinei J, Homma S, Jiang X-C, Abel ED, Goldberg IJ.** 2008. Ceramide is a cardiotoxin in lipotoxic cardiomyopathy. J. Lipid Res. **49:**2101–2112. http://dx.doi.org/10.1194/jlr.M800147-JLR200.
43. **Shen E, Li Y, Li Y, Shan L, Zhu H, Feng Q, Arnold JM, Peng T.** 2009. Rac1 is required for cardiomyocyte apoptosis during hyperglycemia. Diabetes **58:**2386–2395. http://dx.doi.org/10.2337/db08-0617.
44. **Li J, Zhu H, Shen E, Wan L, Arnold JM, Peng T.** 2010. Deficiency of rac1 blocks NADPH oxidase activation, inhibits endoplasmic reticulum stress, and reduces myocardial remodeling in a mouse model of type 1 diabetes. Diabetes **59:**2033–2042. http://dx.doi.org/10.2337/db09-1800.
45. **Roe ND, Thomas DP, Ren J.** 2011. Inhibition of NADPH oxidase alleviates experimental diabetes-induced myocardial contractile dysfunction. Diabetes. Obes. Metab. **13:**465–473. http://dx.doi.org/10.1111/j.1463-1326.2011.01369.x.
46. **Cave A, Grieve D, Johar S, Zhang M, Shah AM.** 2005. NADPH oxidase-derived reactive oxygen species in cardiac pathophysiology. Philos. Trans. R. Soc. Lond. B Biol. Sci. **360:**2327–2334. http://dx.doi.org/10.1098/rstb.2005.1772.
47. **Boni LT, Rando RR.** 1985. The nature of protein kinase C activation by physically defined phospholipid vesicles and diacylglycerols. J. Biol. Chem. **260:**10819–10825.
48. **Bourbon NA, Yun J, Kester M.** 2000. Ceramide directly activates protein kinase C ζ to regulate a stress-activated protein kinase signaling complex. J. Biol. Chem. **275:**35617–35623. http://dx.doi.org/10.1074/jbc.M007346200.
49. **Inoguchi T, Battan R, Handler E, Sportsman JR, Heath W, King GL.** 1992. Preferential elevation of protein kinase C isoform βII and diacylglycerol levels in the aorta and heart of diabetic rats: differential reversibility to glycemic control by islet cell transplantation. Proc. Natl. Acad. Sci. U. S. A. **89:**11059–11063. http://dx.doi.org/10.1073/pnas.89.22.11059.
50. **Xia Z, Kuo K-H, Nagareddy PR, Wang F, Guo Z, Guo T, Jiang J, McNeill JH.** 2007. *N*-Acetylcysteine attenuates PKCβ2 overexpression and myocardial hypertrophy in streptozotocin-induced diabetic rats. Cardiovasc. Res. **73:**770–782. http://dx.doi.org/10.1016/j.cardiores.2006.11.033.
51. **Guo Z, Xia Z, Jiang J, McNeill JH.** 2007. Downregulation of NADPH oxidase, antioxidant enzymes, and inflammatory markers in the heart of streptozotocin-induced diabetic rats by *N*-acetyl-L-cysteine. Am. J. Physiol. Heart Circ. Physiol. **292:**H1728–H1736. http://dx.doi.org/10.1152/ajpheart.01328.2005.
52. **Liu Y, Lei S, Gao X, Mao X, Wang T, Wong GT, Vanhoutte PM, Irwin MG, Xia Z.** 2012. PKCβ inhibition with ruboxistaurin reduces oxidative stress and attenuates left ventricular hypertrophy and dysfunction in rats with streptozotocin-induced diabetes. Clin. Sci. (Lond.) **122:**161–173. http://dx.doi.org/10.1042/CS20110176.
53. **Okumura K, Akiyama N, Hashimoto H, Ogawa K, Satake T.** 1988. Alteration of 1,2-diacylglycerol content in myocardium from diabetic rats. Diabetes **37:**1168–1172. http://dx.doi.org/10.2337/diab.37.9.1168.
54. **Koya D, King GL.** 1998. Protein kinase C activation and the development of diabetic complications. Diabetes **47:**859–866. http://dx.doi.org/10.2337/diabetes.47.6.859.
55. **Pulinilkunnil T, Kienesberger PC, Nagendran J, Waller TJ, Young ME, Kershaw EE, Korbutt G, Haemmerle G, Zechner R, Dyck JRB.** 2013. Myocardial adipose triglyceride lipase overexpression protects diabetic mice from the development of lipotoxic cardiomyopathy. Diabetes **62:**1464–1477. http://dx.doi.org/10.2337/db12-0927.
56. **Ueno M, Suzuki J, Zenimaru Y, Takahashi S, Koizumi T, Noriki S, Yamaguchi O, Otsu K, Shen W-J, Kraemer FB, Miyamori I.** 2008. Cardiac overexpression of hormone-sensitive lipase inhibits myocardial steatosis and fibrosis in streptozotocin diabetic mice. Am. J. Physiol. Endocrinol. Metab. **294:**E1109–E1118. http://dx.doi.org/10.1152/ajpendo.00016.2008.
57. **Newton AC.** 2009. Lipid activation of protein kinases. J. Lipid Res. **50:**S266–S271. http://dx.doi.org/10.1194/jlr.R800064-JLR200.
58. **Ishii H, Jirousek MR, Koya D, Takagi C, Xia P, Clermont A, Bursell SE, Kern TS, Ballas LM, Heath WF, Stramm LE, Feener EP, King GL.** 1996. Amelioration of vascular dysfunctions in diabetic rats by an oral PKCβ inhibitor. Science **272:**728–731. http://dx.doi.org/10.1126/science.272.5262.728.
59. **Wakasaki H, Koya D, Schoen FJ, Jirousek MR, Ways DK, Hoit BD, Walsh RA, King GL.** 1997. Targeted overexpression of protein kinase C β2 isoform in myocardium causes cardiomyopathy. Proc. Natl. Acad. Sci. U. S. A. **94:**9320–9325. http://dx.doi.org/10.1073/pnas.94.17.9320.
60. **Brose N, Rosenmund C.** 2002. Move over protein kinase C, you've got company: alternative cellular effectors of diacylglycerol and phorbol esters. J. Cell Sci. **115:**4399–4411. http://dx.doi.org/10.1242/jcs.00122.
61. **Duncan JG.** 2011. Mitochondrial dysfunction in diabetic cardiomyopathy. Biochim. Biophys. Acta **1813:**1351–1359. http://dx.doi.org/10.1016/j.bbamcr.2011.01.014.
62. **Park JW, Hoyal CR, Benna JE, Babior BM.** 1997. Kinase-dependent activation of the leukocyte NADPH oxidase in a cell-free system. Phosphorylation of membranes and $p47^{PHOX}$ during oxidase activation. J. Biol. Chem. **272:**11035–11043.
63. **Kunisaki M, Bursell SE, Umeda F, Nawata H, King GL.** 1994. Normalization of diacylglycerol-protein kinase C activation by vitamin E in aorta of diabetic rats and cultured rat smooth muscle cells exposed to elevated glucose levels. Diabetes **43:**1372–1377. http://dx.doi.org/10.2337/diab.43.11.1372.
64. **Atsumi H, Kitada M, Kanasaki K, Koya D.** 2011. Reversal of redox-dependent inhibition of diacylglycerol kinase by antioxidants in mesangial cells exposed to high glucose. Mol. Med. Rep. **4:**923–927. http://dx.doi.org/10.3892/mmr.2011.524.